Energy Equip. Sys./ Vol. 6/No. 1/March 2018/ 51-59

ENERGY EQUIPSYS

Energy Equipment and Systems

http://energyequipsys.ut.ac.ir
www.energyequipsys.com

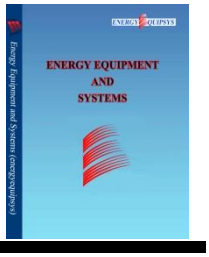

Stochastic reconstruction of carbon fiber paper gas diffusion layers of PEFCs: A comparative study

Authors

Sepehr Sima Afrookhteh [a]
Jalil Jamali *[b]
Mohsen Shakeri[c]
Majid Baniassadi [d]

[a] Renewable Energy Research Center, Mechanical Engineering Department, Babol Noshirvani University of Technology, Babol, Iran

[b] Department of Mechanical Engineering, Shoushtar Branch, Islamic Azad University, Shoushtar, Iran

[c] Fuel cell research and Technology center, Mechanical Dept. Babol Noshirvani University of Technology, babol , Mazandaran

[d] School of Mechanical Engineering, University of Tehran, Tehran, Iran

Article history:

Received : 8 September 2017
Accepted : 16 September 2017

ABSTRACT

A 3D microstructure of the non-woven gas diffusion layers (GDLs) of polymer electrolyte fuel cells (PEFCs) is reconstructed using a stochastic method. For a commercial GDL, due to the planar orientation of the fibers in the GDL, 2D SEM image of the GDL surface is used to estimate the orientation of the carbon fibers in the domain. Two more microstructures with different fiber orientations are generated and compared. The method is verified by comparing the commercial GDL (Toray TGP-H-060) model properties with other simulations or real GDL data. Three different reconstructed models are compared in terms of permeability, and the 3D pore size distribution of the models is also investigated. Through-plane (TP) and in-plane (IP) tortuosity, and the effects of binder addition on tortuosity are also discussed. For the TGH-H-060, tortuosity is derived to be 0.93, 1.50, and 1.42 in IP-x, IP-y, and TP-z directions, respectively. It is shown that adding binders to the fibrous skeleton increases the tortuosity of the pore phase.

Keywords: GDL Reconstruction, Fiber Orientation, Pore Size Distribution, Permeability, Tortuosity

1. Introduction

Fuel cells are electrochemical devices that convert the chemical energy of fuels into electrical energy. An ideal option for a wide variety of portable, stationary, and automotive applications[1] is using the polymer electrolyte fuel cells due to their modular design, high efficiency, and environmental benefits. The gas diffusion layer is a multifunctional, thin, and porous layer that provides a pathway for reactant gases and the produced water. GDLs also electrically connect the bipolar plate and the catalyst layer, and remove the resulting heat of electrochemical reactions. The compressibility of the GDLs also protects the membrane electrode assembly (MEA) from mechanical stresses, thus preventing the MEA from sagging into the flow field channels [2].

Porous carbon fiber papers are one of the most interesting materials which can maintain the GDLs' conflicting functions. There are many different types of commercially available carbon fiber paper used as a gas diffusion layer in the fuel cell industry with a wide range of

* Corresponding author: Jalil Jamali
Department of Mechanical Engineering, Shoushtar Branch, Islamic Azad University, Shoushtar, Iran
Email: ja_ja032@yahoo.com

thicknesses from 110 to 400 micrometer and 75–88% porosity [2, 3]. GDLs are usually comprised of carbon fibers and a carbonaceous binder. Polytetrafluoroethylene (PTFE) is applied to some commercial GDLs to enhance the hydrophobicity of the porous media. Every structural parameter, namely porosity, thickness, fiber diameter, and binder/PTFE content, can influence the microstructure and the final performance of the GDL in a fuel cell system. Hence, obtaining a modifiable 3D microstructure model can help researchers in studying the effects of interrelated parameters and mass transport properties in a fast and flexible manner.

Two methods can be employed to reconstruct the 3D microstructure of GDLs [4, 5]. The first is imaging-based methods such as X-ray micro/nano-tomography which capture a series of 2D images at different angles of the same axis of rotation and combine the 2D images using computer software [6–9]. The second method involves using stochastic approaches to generate digital models [10–14]. Imaging-based methods are expensive, and large data volumes and the difficulty of analysis are their major disadvantageous. But digital stochastic modeling approaches are cheap and easy to implement. Besides, the reconstructed models are modifiable and can be altered for further investigation.

In terms of stochastic modeling, Wu et al. [14] reconstructed the microstructure of catalyst layers and non-woven GDLs of the PEFCs using a non-uniform sphere-based simulated annealing approach. They performed characterization analysis to obtain structural properties and developed a Lattice Boltzmann method to calculate effective mass transport properties of the microstructures. In a recent work, Tayarani et al. [15] developed the GDL 3D microstructure using stochastic approaches. They simulated transport properties of the GDLs under different ranges of PTFE loadings and water saturation levels (dry and wet conditions), and validated their results through experimental data and empirical formulations. Most of the presented methods for carbon fiber generation in the literature [5, 13, 15, 16] are adapted from a stochastic generation technique developed by Schladitz et al. [17]. In their method, the carbon fibers density is a function of fiber directions in the x–y plane. They introduced an anisotropic parameter (β), while increasing β makes the fibers increasingly parallel to the x–y plane. Another important component of the GDL microstructure is the carbonaceous binder, but only a few papers incorporated the binder to carbon fibers [4]. There are different methods for digitally adding a binder to the fibrous skeleton [15, 18]. But image processing techniques using morphological operators [7, 19, 20] seem to be an effective way to model the binder as a wetting fluid that mainly accumulates at the fiber intersections.

In the present study, a stochastic method is used to generate a fibrous substrate of the non-woven carbon fiber paper GDLs. Using SEM image of a commercial GDL, the 3D microstructure of the material is reconstructed. Two different virtual microstructures are generated to investigate the effects of fiber distribution on the mass transport properties of the GDLs. The pore size distribution of all models is extracted in 3D, and the effect of binder addition on the tortuosity of the models is evaluated and discussed.

2. Modeling procedure

2.1. Generating three stochastic microstructure

The modeling is based on the TGP-H-060 (Toray, Japan), a commercially available GDL, with 78% porosity and 190 μm of thickness. This type of GDL has no PTFE treatment and microporous layer. Using surface SEM image of the GDL, as shown in Fig. 1, the average diameter of the fibers is measured on the SEM image as equal to 7 μm. The following assumptions are made to simplify the GDL modeling methodology: All fibers are straight and cylindrical with a constant radius, the fiber length is equal to the sample size, and overlapping between fibers is allowed. A MATLAB code is developed to generate stochastic fibers in space. The coordinates of the head point of each individual cylinder (carbon fiber) are selected randomly in the working domain in the following manner:

$$x_1 = x_0 + \mathrm{LCos}\theta \tag{1}$$

$$y_1 = y_0 + \mathrm{LSin}\theta \tag{2}$$

$$z_1 = z_0 \tag{3}$$

where L is the length of the fibers and is equal to the sample size, and θ is the orientation angle of the fibers in the x–y plane. Eq.3 is considered due to the manufacturing process and the planar orientation of the GDL fibers. The orientation distribution of the real GDL fibers in Fig. 1 is calculated and quantified using an open source code, ImageJ [21]. The

(a)

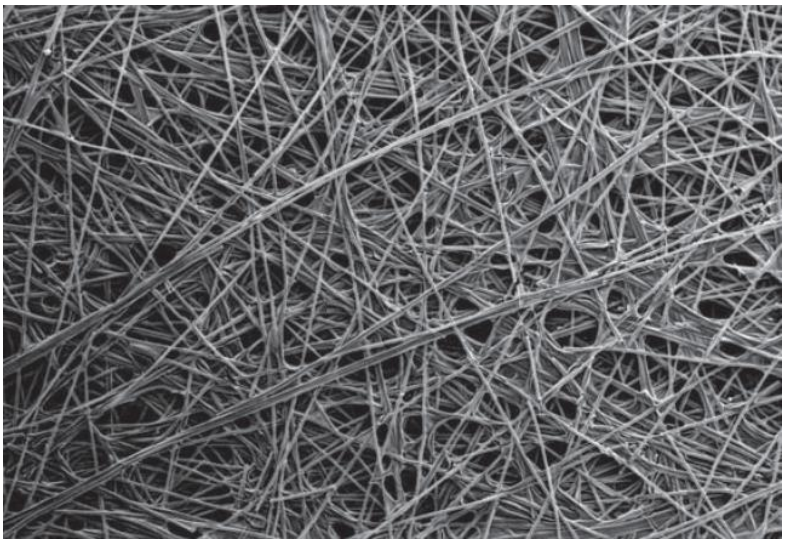

(b)

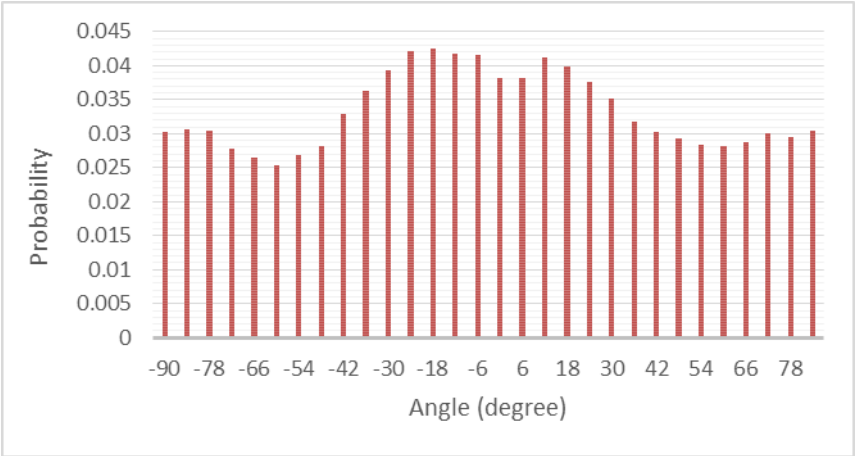

Fig. 1. a) Surface SEM image of the Toray TGP-H-060 [3], b) Orientation distribution of carbon fibers in Case A, obtained by directionality measurements in ImageJ

result of the orientation distribution measurement is illustrated in Fig. 2. The quantified orientation of fibers in the real SEM image is then applied to the fiber-generating algorithm using a fitness proportionate selection method.

Two more microstructures are reconstructed virtually using the same method. The constant parameters of the three models are shown in Table 1. The orientation of fibers on the plane is the only parameter that is different in these three cases. For virtual microstructures (Cases B and C), the occurrence probability of each angle is presented in Table 2.

2.2. Binder addition

During the papermaking process, the carbon fibers are dispersed in a water and binder (usually polyvinyl alcohol) solution. During the solvent evaporation step, the binder mostly accumulates at the fiber intersection due to their low static contact angle on the fibers [15, 22]. To mimic this procedure, image processing techniques are used to add the binder to the carbon fiber substrate. A morphological operator of opening [19] is implemented using AVIZO Fire on three microstructures. A binder usually constitutes 27–45 volume percentage of the final GDL structure solid phase. Here, for all cases, it is assumed that the binder constitutes 40% of solid volume fraction. To

compute the total fiber count (n) in the domain, the following formulation is considered:

$$V_{fibers} = \frac{1-\varepsilon- B_{svp}}{V_d} \quad (4)$$

$$n = \frac{V_{fibers}}{V_f} \quad (5)$$

where ε is porosity and B_{svp} is the binder solid volume percentage. V_{fibers} and V_f are the volume of all solid fibers in the domain and the volume of an individual fiber, respectively, and V_d is the volume of the working domain. Since the volume percentage of the binder is considered in the fiber count calculation, higher porosity is obtained for naked fibers. Thus, morphological opening is applied to the pore phase with an appropriate shape and size of the structuring element (SE) [19] to achieve the final desired porosity. Ball (spherical) SEs seem to be the most appropriate structuring element to mimic the wetting nature of the binder [7, 20]. Three generated microstructures are shown in Fig. 2. The applied orientation of the fibers depicted in Table 2 can be visually inspected in Cases B and C (Figs. 2b and 2c)

Table 1. Constant input parameters for three different microstructures.

Carbon fiber paper	Fiber diameter (μm)	Porosity	Thickness (μm)	Binder volume percentage of solid phase (%)	Bulk density (g/cm^3)	Domain size (μm^3)
Non-woven	7	0.78	190	40	0.44	300×300×190

Table 2. Fiber orientation distribution in Cases B and C.

Angles (degree)		-90	-45	-30	0	30	45	90
Probability of occurrence	*Case B*	0	0.5	0	0	0	0.5	0
	Case C	0.2	0	0.2	0.2	0.2	0.2	0

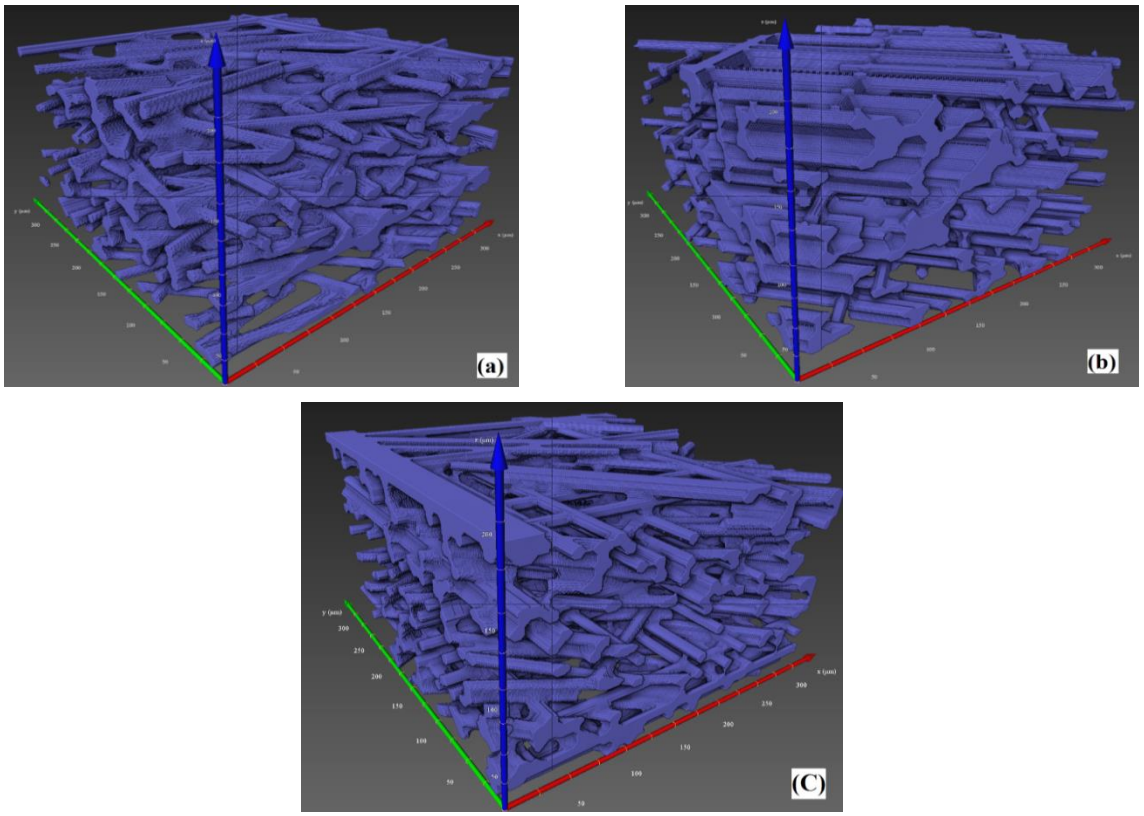

Fig. 2. 3D representation of reconstructed GDLs; (a) Case A (Toray-TGP-H-060), (b) Case B, (c) Case C, light blue color represents solid phase (fibers + binder), and the pore phase is transparent.

3. Results and discussion

3.1. Microstructure validation and characterization

To validate the proposed methodology and the resultant microstructure, structural validation and comparison between structural parameters are conducted. In the binder addition step, an attempt was made to reach the closest value to the desired porosity, and since the porosity of fibers without the binder was different in each case, different sizes of ball SEs are tried. The values are presented in Table 3. These results show that the desired porosity (78%) after binder addition is reached in almost all cases.

The 2D representations of the reconstructed microstructure before and after the binder addition are shown in Fig. 4. The correct distribution of the binder can be inspected visually by comparing the digital microstructure before and after the binder addition. The same 2D slice of the reconstructed microstructure of Case A is shown, and it is obvious that the binder quite expectedly mostly accumulated at fiber intersections and filled the small pores. This confirms the correct binder distribution and the method used for digital binder impregnation.

In the next step, the 3D pore size distribution of the microstructures is characterized. The volume of each 3D pore (sphere) is measured and the equivalent diameter of the pores is obtained using the AVIZO Fire (FEI, France) software. For comparison purposes, the PSDs of all three microstructures are computed on a 200×200×190 μm^3 domain, and the results are presented in Fig. 4. The mean pore diameter for Cases A, B, and C are 35, 35, and 34 μm, respectively. The mean pore diameter of Case A is in the range of 30–40 μm, as reported by Mathias [22] for the TGP-H-060. For a greater validation of our methodology, Case A is compared with other simulations on the Toray TGP-H in terms of PSD. Hannach and Kjeang [23] reported the minimum and mean pore size of the Toray TGP-H paper for 200×200×170 μm^3 domain size around 1 and 30 μm, respectively, which compares favorably with results presented in Fig. 5a. For the TGP-H-060, Wu's [14] simulations resulted in an equivalent diameter of pores in the range of ~ 1.5–50 μm, which is the same as the results of Fig. 4a. The diameter of pores in all cases are in good accordance with the range of pore diameter for commercial GDLs (1–150μm)[24]. It should be noted that, as it is shown in Fig. 4, most of the pore diameters lie below 50 μm in all cases, and since the pores' >50 μm diameter can negatively affect mass transport properties of the GDLs [14], two virtual GDLs (Cases B and C) can be selected for fuel cell applications.

Table 3. Porosity of reconstructed microstructures prior and after binder addition.

Case	Porosity of fibrous skeleton (%)	Ball SE size (px)	Porosity after binder addition (%)
A	84.4	6	78.5
B	86.1	7	79.6
C	83.1	5	77.9

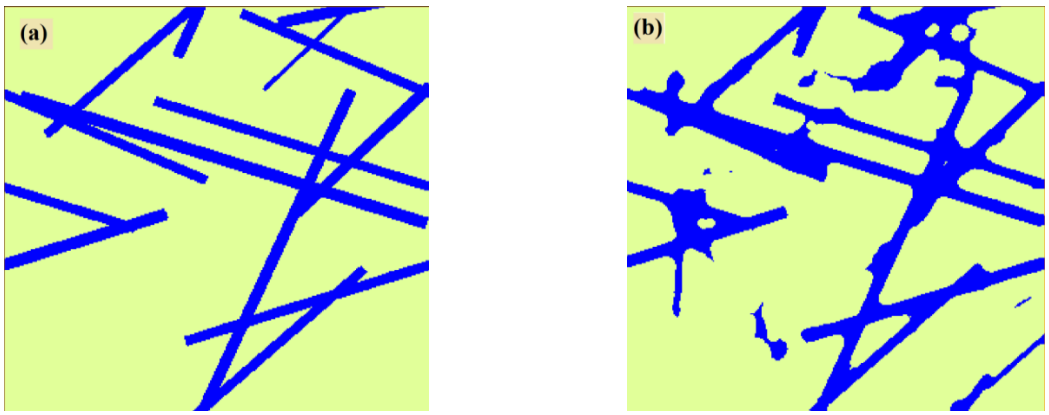

Fig. 3. The same 2D slice of the reconstructed GDL of Case A: (a) before binder addition, (b) after binder addition. Blue color represents solid phase and the rest is the pore phase of the microstructure.

The tortuosity factor (τ_f) is another important characteristic of a porous medium and geometrically is the fraction of the tortuous path length to the shortest path length in the flow transport direction. Different methods are used in the literature to measure this parameter, but using heat transfer and effective thermal conductivity equations provides an adequate approach [25]:

$$V_{fibers} = \frac{1-\varepsilon - B_{svp}}{V_d} \quad (6)$$

where k_{eff} is the effective thermal conductivity of the void phase, and it can be measured by solving Fourier equations and using finite volume method in the AVIZO Fire software. k_{bulk} is the bulk thermal conductivity of the void phase and is considered to be 0.026 W/m.K for air in the void phase [15].

(a)

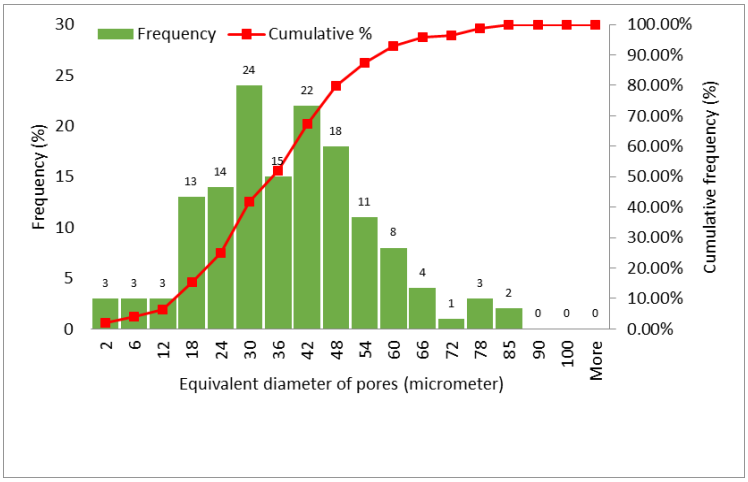

(b)

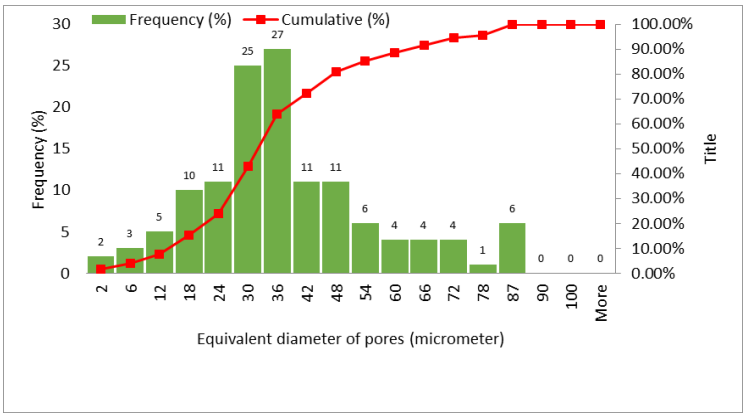

(c)

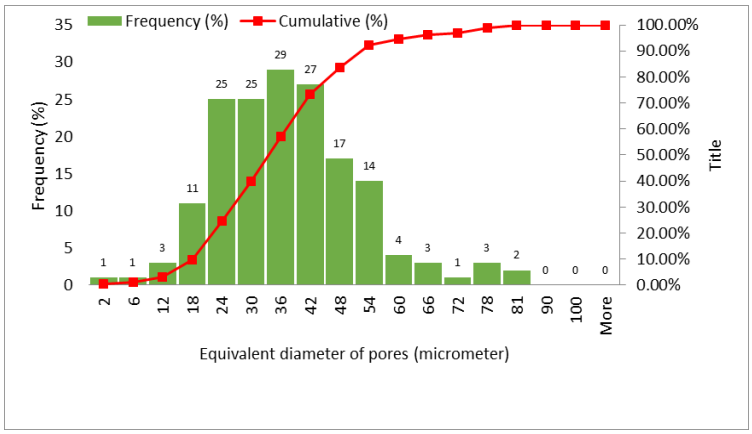

Fig. 4. Pore size distribution of the reconstructed models on a 200×200×190 μm^3 domain: (a) Case A, (b) Case B, and (c) Case C.

Table 4. Through-plane tortuosity factor prior and after binder addition.

Microstructures	Through-plane tortuosity factor					
	Before binder addition			After binder addition		
	x	***y***	***z***	***x***	***y***	***z***
Case A	0.82	1.16	1.13	0.93	1.50	1.42
Case B	0.78	1.18	1.10	0.95	1.50	1.32
Case C	1.05	1.22	1.23	1.25	1.59	1.55

The results of the tortuosity factor computation are shown in Table 4. The tortuosity factor of the Toray TGP-H-060 was numerically calculated by Didari et al. [26] and it was derived to be 1.85 in the TP direction. Although our result is in good agreement with the literature [14, 27], where 1.2–1.4 TP tortuosity for 78% porous TGP-H-060 is derived through the Lattice Boltzmann method, the discrepancy between the result of this paper and that calculated in [26] can be due to the different input parameters. In contrast to our study, they considered 200 μm of thickness and 0.27 solid fraction of a carbonaceous thermoset binder for the Toray TGP-H-060 carbon paper GDL. Tortuosity values in Cases B and C show higher values than in Case A, meaning more tortuous pathways in these cases. As is obvious in Table 4, the tortuosity factor in all cases and all directions increased after binder addition. This can be mainly attributed to the decrease in porosity and the increase in the solid volume fraction after the binder addition, which can cause the pathways to deviate from straight lines and become more tortuous.

3.2. Mass transport characterization

The mass transport property of the reconstructed model is also investigated through permeability measurements. Permeability (K) is a microstructure-dependent property of a porous medium and is the ability of the structure to transport a fluid flow (Q) under a pressure gradient ($\Delta P/L$) and is usually defined by Darcy's law:

$$Q = \frac{KA}{\mu}\frac{\Delta P}{L} \tag{7}$$

where μ is the dynamic viscosity and is equal to 1.85×10^{-5} Pa.s for air, and A is the cross section of the material in the flow direction. To investigate the mass transport property of the models, absolute (single-phase) permeability in the TP and the direction in all cases are computed. For this computation, Navier–Stokes equations are simplified and solved using a finite volume method. The equations are solved using a volume-averaging [28] method in the entire volume. The flow is considered laminar, Newtonian, and incompressible. The assumption of a steady-state flow is also made. Calculations conducted on the models at five different $150\times150\times190$ μm^3 regions of interest in the working domain using a volume-averaging method in the AVIZO and the mean value are reported in Fig. 5. The range of permeability of the TGP-H-060 is reported to be between 5 and 10 μm^2 in the literature [22, 26, 27]. Since the number of binders in the final microstructure is not reported in much of the literature, a higher value of TP permeability of Case A in this work can be explained by different amounts of binder materials in our assumptions. The different values of permeability in Cases B and C may be due to the predefined orientation of the fibers. It can be concluded that the fiber orientation of the GDLs has a decisive effect on the different properties of the GDLs.

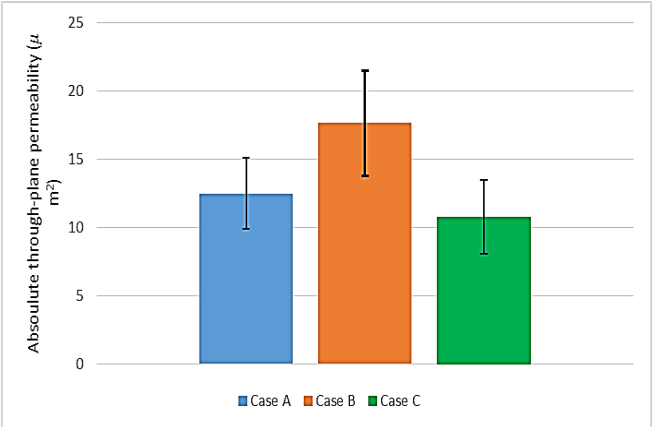

Fig. 5. Absolute through-plane permeability of three cases with constant porosity ($\boldsymbol{\varepsilon = 0.78}$)

4. Conclusion

The microstructure of a PEFC gas diffusion layer was reconstructed using a stochastic method. All solid phases of a commercial GDL, including carbon fibers and binders, are digitally modeled. The accuracy of the method was appraised through a comparison of the

tortuosity and pore size distribution of the model of commercial GDL in the literature. The mean pore radius of the TGP-H-060 was computed to be 35 μm, which was in the range reported in the literature. In terms of mass transport properties of the model, permeability of the models was calculated in the TP direction and the effect of fiber orientation of the TP permeability was shown. An advantage of the proposed approach is the ability to obtain the tortuosity of the GDL, which is an anisotropic material, before and after binder addition, and in all directions. The method used here is flexible and capable of modeling carbon fiber GDLs with different porosity, fiber radii and orientations, and GDLs with different binder volume percentages can be modeled and characterized quickly and accurately. Finally, it was shown that engineering the microstructure of the GDLs, especially fiber orientation, can inherently change its mass transport characterizations, which can directly influence the performance of the fuel cell.

References

[1] Wang Y., A Review of Polymer Electrolyte Membrane Fuel Cells, Technology, Applications, and Needs on Fundamental Research, Applied Energy (2011) 88(4):981-1007.

[2] Barbir F., PEM Fuel Cells, Theory and Practice (2013) Academic Press.

[3] Wilkinson D.P., Proton Exchange Membrane Fuel Cells, Materials Properties and Performance (2009) CRC Press.

[4] Fadzillah D.M., Review on Microstructure Modelling of a Gas Diffusion Layer for Proton Exchange Membrane Fuel Cells, Renewable and Sustainable Energy Reviews (2016).

[5] Shojaeefard M.H., A Review on Microstructure Reconstruction of PEM Fuel Cells Porous Electrodes for Pore Scale Simulation, International Journal of Hydrogen Energy (2016) 41(44): 20276-20293.

[6] James J.P., Choi H.W., Pharoah J.G., X-Ray Computed Tomography Reconstruction and Analysis of Polymer Electrolyte Membrane Fuel Cell Porous Transport Layers, International Journal of Hydrogen Energy (2012)37(23): 18216-18230.

[7] Becker J., Determination of Material Properties of Gas Diffusion Layers, Experiments and Simulations Using Phase Contrast Tomographic Microscopy, Journal of The Electrochemical Society (2009)156(10): B1175-B1181.

[8] Fishman Z., Hinebaugh J., Bazylak A., Microscale Tomography Investigations of Heterogeneous Porosity Distributions of PEMFC GDLs, Journal of the Electrochemical Society (2010) 157(11): B1643-B1650.

[9] Ostadi H., 3D Reconstruction of a Gas Diffusion Layer and a Microporous Layer, Journal of Membrane Science (2010) 351(1–2): 69-74.

[10] Baniassadi M., Three-Dimensional Reconstruction and Homogenization of Heterogeneous Materials Using Statistical Correlation Functions and FEM, Computational Materials Science (2012) 51(1): 372-379.

[11] Sheidaei A., 3-D Microstructure Reconstruction of Polymer Nano-Composite Using FIB–SEM and Statistical Correlation Function, Composites Science and Technology (2013) 80: 47-54.

[12] Hinebaugh J., Bazylak A., Stochastic Modeling of Polymer Electrolyte Membrane Fuel Cell Gas Diffusion Layers – Part 1: Physical Characterization, International Journal of Hydrogen Energy (2017).

[13] Yiotis A.G., Microscale Characterisation of Stochastically Reconstructed Carbon Fiber-Based Gas Diffusion Layers, Effects of Anisotropy and Resin Content, Journal of Power Sources (2016)320: 153-167.

[14] Wu W., Jiang F., Microstructure Reconstruction and Characterization of PEMFC Electrodes, International Journal of Hydrogen Energy (2014) 39(28): 15894-15906.

[15] Tayarani-Yoosefabadi Z., Stochastic Microstructural Modeling of Fuel Cell Gas Diffusion Layers and Numerical Determination of Transport Properties in Different Liquid Water Saturation Levels, Journal of Power Sources (2016) 303: 208-221.

[16] Mukherjee P.P., Kang Q., Wang C.-Y., Pore-Scale Modeling of Two-Phase Transport in Polymer Electrolyte Fuel Cells-Progress and Perspective, Energy & Environmental Science (2011) 4(2): 346-369.

[17] Schladitz K., Design of Acoustic Trim Based on Geometric Modeling and Flow Simulation for Non-Woven, Computational Materials Science (2006) 38(1): 56-66.

[18] Thiedmann R., Stochastic 3D Modeling of the GDL Structure in PEMFCs Based on Thin Section Detection, Journal of the Electrochemical Society (2008)155(4): B391-B399.

[19] Ohser J., Schladitz K., 3D Images of Materials Structures: Processing and Analysis (2009)Wiley.

[20] Hinebaugh J., Gostick J., Bazylak A., Stochastic Modeling of Polymer Electrolyte Membrane Fuel Cell Gas Diffusion Layers – Part 2, A Comprehensive Substrate Model with Pore Size Distribution and Heterogeneity Effects, International Journal of Hydrogen Energy (2017).

[21] Schneider C.A., Rasband W.S., Eliceiri K.W., NIH Image to Image J, 25 years of Image Analysis, Nat Meth (2012) 9(7): 671-675.

[22] Mathias M.F., Diffusion Media Materials and Characterisation, In Handbook of Fuel Cells (2010) John Wiley & Sons, Ltd.

[23] El Hannach M., Kjeang E., Stochastic Microstructural Modeling of PEFC Gas Diffusion Media. Journal of The Electrochemical Society (2014) 161(9): F951-F960.
[24] Pant L.M., Mitra S.K., Secanell M., Absolute Permeability and Knudsen Diffusivity Measurements in PEMFC gas Diffusion Layers and Micro Porous Layers, Journal of Power Sources (2012)206: 153-160.
[25] Cooper S.J., Microstructural Analysis of an LSCF Cathode Using in Situ Tomography and Simulation. ECS Transactions (2013)57(1): 2671-2678.
[26] Didari S., Modeling of Composite Fibrous Porous Diffusion Media. International Journal of Hydrogen Energy (2014)39(17): 9375-9386.
[27] Hao L., Cheng P., Lattice Boltzmann Simulations of Anisotropic Permeabilities in Carbon Paper Gas Diffusion Layers, Journal of Power Sources (2009)186(1): 104-114.
[28] Whitaker S., The Method of Volume Averaging (2013) Springer Netherlands.